

# Quenchable Porous High-Temperature Polymorph of Sodium Imidazolate, Nalm

Sanja Burazer, Koen Robeyns, Laure Guénée, Gregor Mali, Fabrice Morelle, Voraksmy Ban, Teodoro Klaser, Yaroslav Filinchuk, Radovan Černý, and Jasminka Popović\*



Cite This: *Cryst. Growth Des.* 2021, 21, 770–778



Read Online

ACCESS |



Metrics & More

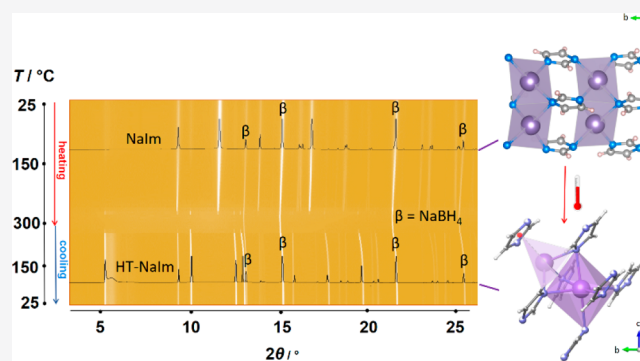


Article Recommendations



Supporting Information

**ABSTRACT:** The novel high-temperature polymorph of sodium imidazolate reported in this paper was discovered in the mechanochemical reaction of NaIm with NaBH<sub>4</sub> and later prepared directly by thermal treatment of the room-temperature polymorph of NaIm. Solid-state NMR was used for initial elucidation of structural features; the crystal structure was determined by single-crystal X-ray diffraction, while the *in situ* HT-XRPD experiments utilizing synchrotron radiation have been performed in order to gain the insight into the structural evolution and thermal stability, in addition to differential thermal analysis and hot-stage microscopy measurements. Contrary to the RT polymorph that forms a dense and hypercoordinated structure without pores, the high-temperature polymorph of NaIm exhibits pores of 50 Å<sup>3</sup> that suggest possible application for gas sorption/separation. It is important to highlight that, once formed, the high-temperature polymorph of NaIm retains its structure and remains stable at room temperature.



## INTRODUCTION

One of the greatest challenges of the 21st century is to create a sustainable and carbon-free energy system capable of meeting today's increased energy demands. Hydrogen, which conveniently can be produced from renewable energy and water, is recognized as the energy carrier of the future, while the major challenge is related, in fact, to the safe and efficient means of storage. Solid-state storage, in particular, the chemical bonding in crystalline compounds, has the greatest potential to fulfill this challenge. On the road to the final transition toward the clean energy society, battery-based research as well as further development of efficient sorption materials deserves a special focus. Metal organic frameworks (MOFs), due to their ultrahigh porosity and huge internal surface areas, together with the enormous degree of variability for both the organic and inorganic components emerged at the top of the list in mentioned applications. Among different classes of MOFs, zeolitic imidazolate frameworks (ZIFs), structured by tetrahedrally configured transition metal cations bridged by imidazolate (Im), represent a particularly wide structural platform able to reproduce the zeolitic topology but also incorporate the electronic properties of the transition metal ions.<sup>1,2</sup>

One of the lately reported ZIFs, ZIF-412, exceeds the previous cage size record observed in ZIF-100 (32–33 Å) and with cage of 38.1 Å in diameter is able to selectively bind large-sized volatile organic compounds, octane and *p*-xylene.

Together with the hydrophobicity, this large pore space provides for exceptionally high separation and cycling performance, especially in the presence of water.<sup>3</sup>

Imidazolate, allowing various connectivity and structural topologies, has also been utilized in novel hybrid materials metal-hydride organic frameworks (HOFs) designed by combining the molecular building blocks of lightweight complex hydrides with organic linkers, where borohydride anions offer an additional functionality.<sup>4–10</sup> The first ever reported HOF, lithium imidazolate-borohydride, Li<sub>2</sub>(Im)BH<sub>4</sub>, was recently synthesized starting from lithium imidazolate and lithium borohydride. Its structure revealed some interesting coordination modes of both anions toward lithium but failed to exhibit any pronounced porosity.<sup>11</sup> A deeper understanding of HOF's fundamental properties has been realized in another study focused on reorientational dynamics of borohydride in the derivative compound lithium benzimidazolate-borohydride Li<sub>2</sub>(bIm)BH<sub>4</sub>.<sup>12</sup>

The initial intention of our research was to obtain Na<sub>2</sub>(Im)BH<sub>4</sub>, the sodium analogue of Li<sub>2</sub>(Im)BH<sub>4</sub>, by

Received: July 21, 2020

Revised: December 17, 2020

Published: January 6, 2021



mechanochemical reaction between NaIm and NaBH<sub>4</sub>. A further analysis will show that the hybrid compound was not obtained; instead, the novel high-temperature polymorph of sodium imidazolate, quenchable down to room temperature (RT), was serendipitously discovered. Despite the fact that the anticipated imidazolate-borohydride compound was not formed, mechanochemically induced crystallization of the new imidazolate phase revealed the new insights into the stability and reactivity of imidazolates depending on the choice of the alkali metal.

As it is well-known, the formation of polymorphs is a very complex phenomenon that depends on the experimental conditions governing the crystallization process. Numerous factors are affecting this process; however, thermodynamics and kinetic aspects of crystallization play the pivotal role. Understanding often the competing, thermodynamic and kinetic factors that govern the formation of different polymorphs helps to facilitate the control over the production of the desired phase, but nevertheless, there are exceptions in practice.<sup>13</sup> From the thermodynamical point of view, any high-temperature (HT) polymorph should be thermodynamically stable only at high temperature, unless it is quenched. Nevertheless, there are many examples where the transition from HT to RT polymorph is hindered by slow kinetics due to high-energy barriers. For example, Androš *et al.* noticed the lack of the transition from the HT phase of Ba<sub>4</sub>Ta<sub>2</sub>O<sub>9</sub> to its RT phase.<sup>14</sup> The fact that the HT phase remains stable at RT probably is related to the particle sizes; particles smaller than some critical size will contribute to the reduced surface free energy of the HT polymorph in respect to the LT structure, thus preventing the polymorphic phase transformation.<sup>15</sup> Another example of size-dependent phase transformation was described by Garvie<sup>16,17</sup> where a high-temperature ZrO<sub>2</sub> phase was also successfully stabilized at room temperature.<sup>14,16</sup> Skoko *et al.* showed that a high-temperature polymorph can be prepared at room temperature by crystallization from different solvents, oxotripropium bromide crystals obtained from dichloromethane, acetone, or chloroform by slow evaporation at room temperature crystallized in HT form.<sup>18</sup>

It is important to highlight that, while ZIFs, a part of the huge family of MOFs, containing a transition metal center and imidazolate anions as bridging linkers, have been extensively studied in literature, the full potential of alkali metal to form MOFs has not been completely explored probably due to the realization that NaIm, KIm, and LiIm form the dense and hypercoordinated structures.<sup>19,20</sup> However, our work demonstrates that the HT polymorph of NaIm, unlike its RT form, exhibits a porous framework structure that suggest the possible application as a solid-state electrolyte or gas sorption/separation material. Moreover, the HT form remains stable upon cooling to RT, which is particularly important application-wise.

## ■ EXPERIMENTAL SECTION

**Synthesis.** Nine mechanochemical reactions of NaBH<sub>4</sub> and NaIm were conducted using the Planetary Micro Mill Fritsch Pulverisette 7 premium line, seven of them as neat grinding (NG), and two of them as liquid-assisted grinding (LAG) with the addition of 50 μL of acetonitrile (ACN) or dimethyl sulfoxide (DMSO). Stainless steel balls (*d* = 5 mm) together with reactants were loaded into a stainless-steel vial (25 mL) under inert conditions. The balls-to-sample mass ratio amounted to 25:1. Ball-milling was performed at 600 rpm (10 min of milling, followed by a 5 min rest time; repeating this procedure

8 times). The reactants and molar ratios used are given in Table S1 (Supporting Information).

Anhydrous sodium borohydride, NaBH<sub>4</sub> (99.99%), was purchased from Sigma-Aldrich, while sodium imidazolate was prepared by the procedure reported elsewhere.<sup>18</sup> Handling and manipulation of the chemicals was performed in an argon-filled glovebox. All solvents have been dried on a vacuum line prior to the utilization in mechanochemical reactors.

**X-ray Powder diffraction (XRPD) at RT.** XRPD measurements at RT were performed on a Stoe IPDS-P diffractometer with monochromated Cu Kα<sub>1</sub> radiation ( $\lambda$  = 1.54060 Å) and a curved image plate detector, in Debye–Scherrer geometry. Air-sensitive samples were mounted in a glovebox in 0.8 mm borosilicate capillaries sealed with vacuum grease. Data were collected in the  $2\theta$  range 2–100° with a counting time of 40 s/step.

**In Situ High-Temperature XRPD.** In situ temperature-dependent XPD was performed using Mo Kα radiation on a Rigaku UltraX S18 generator. The data were collected on a MAR345 image plate and integrated with the program Fit2D.<sup>21</sup> The glass capillaries were heated with a hot air blower, and the rate was set at 15.6 °C/h.

**Solid-State NMR.** NMR measurements were carried out on a 600 MHz Varian NMR system equipped with a 3.2 mm Varian T3 HX MAS probe. Larmor frequencies for <sup>1</sup>H, <sup>13</sup>C, <sup>11</sup>B, and <sup>23</sup>Na were 599.50, 150.74, 192.34, and 158.58 MHz, respectively. <sup>1</sup>H magic angle spinning (MAS) NMR spectra were obtained by using a single 90° pulse excitation (2.3 μs) and sample rotation frequency of 20 kHz. <sup>1</sup>H–<sup>13</sup>C cross-polarization (CP) MAS NMR spectra were recorded by first exciting protons and transferring polarization to carbon nuclei using the amplitude-ramped CP block with a duration of 5 ms. During the acquisition, high-power XiX heteronuclear decoupling was applied; repetition delay was 20 and 480 scans were collected. <sup>11</sup>B MAS NMR spectra were obtained using a short-pulse excitation (0.8 μs) and XiX heteronuclear decoupling during acquisition. Repetition delay was 10 s, and the number of repetitions was 16. <sup>1</sup>H–<sup>11</sup>B CP MAS NMR measurement employed a 0.8 ms CP block and XiX decoupling. Four scans were collected, and the repetition delay was 20 s.<sup>23</sup> Na MAS NMR spectra were also recorded using short-pulse excitation (0.8 μs) and XiX decoupling; the number of scans was 80 and delay between the scans was 10 s. <sup>1</sup>H–<sup>23</sup>Na CP MAS NMR spectra were obtained with a 0.8 ms CP block, repetition delay of 20 s, and 64 collected scans. Frequency axes for <sup>1</sup>H and <sup>13</sup>C NMR spectra were referenced to the corresponding signals of TMS, whereas frequency axes of <sup>11</sup>B and <sup>23</sup>Na spectra were referenced to the signals of H<sub>3</sub>BO<sub>3</sub> and NaCl in solution.

**Synchrotron Radiation X-ray Powder Diffraction (SR-XRPD) at HT.** High-temperature *in situ* powder diffraction (HT-XRPD) data were collected at the beamline BM01, SNBL at the ESRF, Grenoble, France (wavelength  $\lambda$  = 0.8187 Å, sample rotation 0–40°, and X-ray exposure time of 40 s). The samples were mounted in 0.5 mm borosilicate capillaries and closed with vacuum grease. The Dectris Pilatus 2M detector was used for recording 2D powder data at the sample to detector distances of 200 or 400 mm. For integration of the 2D images, the local program Bubble was used.<sup>22</sup> Samples were heated by a heat blower from RT to 300 °C with a 5 °C/min heating rate.

**Single-Crystal X-ray Structural Study.** Single-crystal X-ray data were collected on a Rigaku SuperNova diffractometer equipped with a micro-focus Cu Kα tube and an Atlas CCD detector. Data integration and reduction was performed by CrysAlisPro,<sup>23</sup> and a numerical face-indexed absorption correction was applied. SHELXT<sup>24</sup> was used for structure solution, and refinement was performed by SHELXL<sup>24</sup> against *F*<sup>2</sup>. The structure crystallizes in the chiral space group *P*3<sub>1</sub>12, but was found to be twinned by inversion, with a refined Flack parameter of 0.6. Hydrogen atoms were added on calculated positions with temperature factors fixed at 1.2*U*<sub>eq</sub> of the parent atoms. For the minor part, the imidazolate anions were refined as rigid groups, allowing to rotate around and move with a pivot nitrogen atom.

The figures were made by VESTA<sup>25</sup> or CCDC-Mercury.<sup>26</sup>

**Thermal Analysis.** Differential thermal analysis (DTA) measurements were performed with a Shimadzu DTG-60H analyzer in a

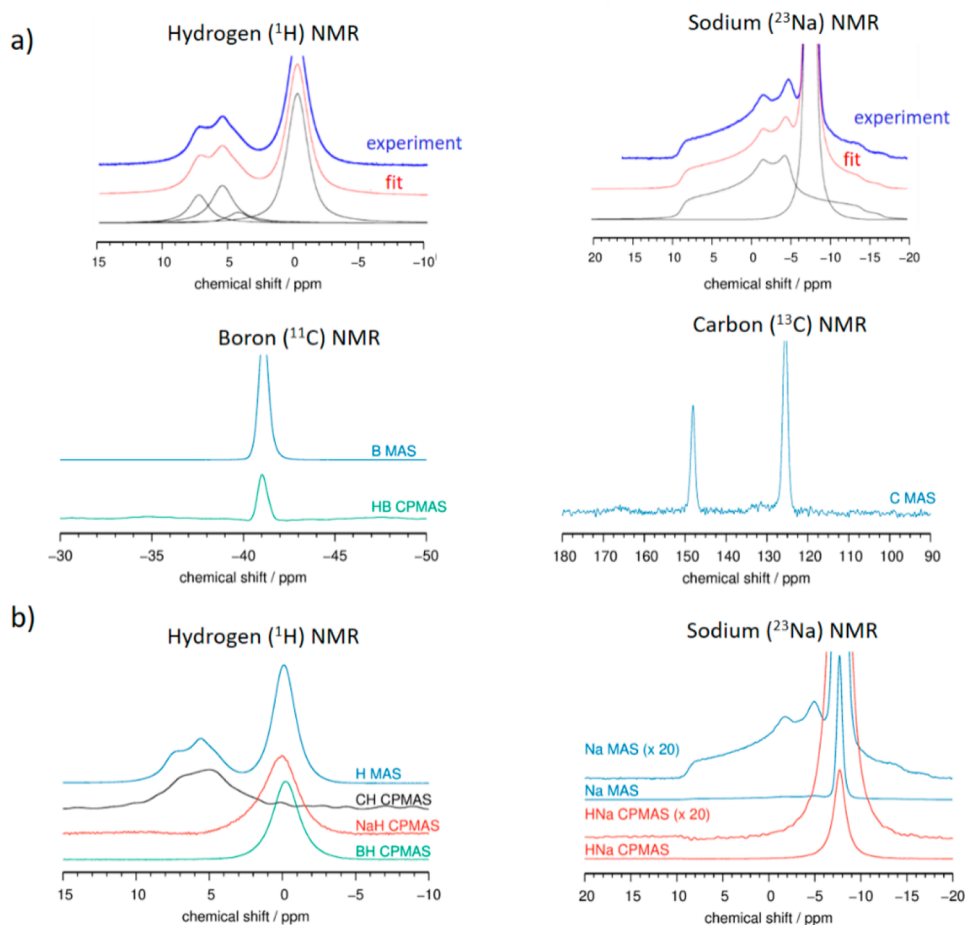


**Figure 1.** (a)  $^1\text{H}$ ,  $^{23}\text{Na}$ ,  $^{11}\text{B}$ , and  $^{13}\text{C}$  NMR spectra for sample D4. (b) Decomposition of the  $^1\text{H}$  and  $^{23}\text{Na}$  MAS NMR spectra.

stream of nitrogen gas in the temperature range from RT to 220 °C with a heating rate of 5 °C min<sup>-1</sup>. Two heating and two cooling runs were measured. Hot-stage microscopy measurements were performed using a Nikon Aclipse LV150NL hot-stage microscope equipped with a Linkam T95-PE camera in the temperature range from RT to 220 °C at a heating rate of 10 °C/min. Changes in crystal morphology and color have been investigated during two heating and two cooling runs.

Differential scanning calorimetry (DSC) analysis was performed on a DSC 821 Mettler instrument in a dynamic nitrogen atmosphere (100 mL·min<sup>-1</sup>) using the heating mode from laboratory temperature to 215 °C and cooling mode from 215 °C to laboratory temperature with a 5 °C min<sup>-1</sup> heating rate. The powder sample was loaded into a crucible under an argon atmosphere and closed with an aluminum pan for the DSC analysis.

## RESULTS AND DISCUSSION

Samples denoted D1–D7 were prepared by the mechanochemical reactions of NaBH<sub>4</sub> and NaIm in 1:6, 1:4, 1:2, 1:1, 2:1, 4:1, and 6:1 molar ratios (Table S1). XRPD patterns of samples D1–D7 (Figure S1) show the presence of starting reactants but also indicate that a new, yet unidentified, crystalline phase forms in all samples. Also, it has been noted that the amount of this phase becomes significant when an excess of imidazolate was used.

**Solid-State NMR Measurements.** In order to gain the insight into the structural composition of the prepared samples, solid-state NMR measurements have been conducted. Measurements have been conducted on the D4 sample since it contains the smallest amount of amorphous phase. The  $^1\text{H}$ ,

$^{13}\text{C}$ ,  $^{23}\text{Na}$ , and  $^{11}\text{B}$  solid-state NMR spectra for the D4 sample are shown in Figure 1.

In proton spectra, four contributions resonating at 7.4, 5.6, 4.4, and -0.1 ppm are observed. From the two-dimensional  $^1\text{H}$ – $^{13}\text{C}$  heteronuclear correlation spectrum (only the projection onto the  $^1\text{H}$  dimension is shown with a black solid line and denoted as CH-CPMAS below the  $^1\text{H}$  MAS spectrum), one can see that only the first three signals are close to carbon nuclei. On the contrary, the  $^1\text{H}$  signal resonating at -0.1 ppm is close to Na and B nuclei; cross-polarization between these H nuclei and Na and B nuclei is efficient as shown by red and green spectra denoted as NaH- and BH-CPMAS, respectively. The lack of the -0.1 ppm proton signal in the CH heteronuclear correlation spectrum suggests that H atoms of this species are far from imidazole (possibly in different domains or crystallites). The sodium spectrum exhibits two very different signals, one narrow and symmetric resonating at about -7 ppm, and one with a typical broad quadrupolar line shape extending between 9 and -16 ppm. The H–Na CPMAS spectrum shows that only the narrow contribution is efficiently cross-polarized from protons. The narrow symmetric line for  $^{23}\text{Na}$  nuclei indicates a highly symmetric position (as in a cubic-like environment) or motionally averaged environment. However, since H–Na cross-polarization works well, motion is probably not very fast. The weaker, broader signal in the Na spectrum belongs to a less symmetric environment, not close to hydrogen atoms. In the boron NMR spectrum, only one symmetric signal can be

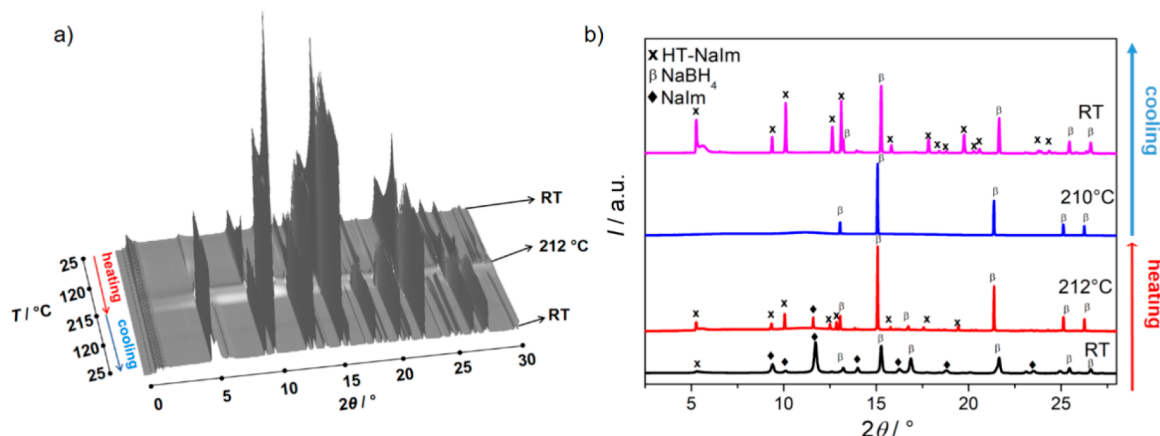


**Figure 2.** (a) XRD patterns of sample D4 collected during a heating run in the temperature range from RT to 240 °C and during cooling back to RT. (b) Phase composition of sample D4 at RT and 212 °C during the heating, and 210 °C and RT during the subsequent cooling run. Diffraction lines belonging to NaIm are marked with diamonds, NaBH<sub>4</sub> with  $\beta$ , and HT-NaIm with x. Wavelength  $\lambda = 0.8187$  Å.

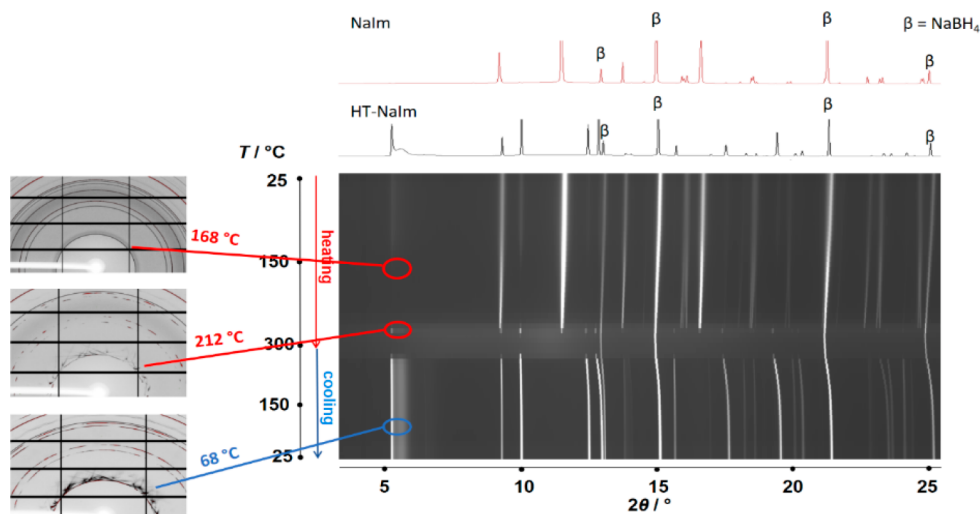


**Figure 3.** XRD patterns of sample D4 collected during heating run in the temperature range from RT to 240 °C and during the cooling run back to RT with diffraction patterns of pure room-temperature NaIm and high-temperature NaIm, as well as diffraction patterns of sample D4, collected at 168 and 212 °C during heating and at 68 °C during cooling.

seen. Since <sup>11</sup>B nuclei are quadrupolar nuclei (like <sup>23</sup>Na, and unlike <sup>1</sup>H), the narrow symmetric line again indicates either a highly symmetric environment or fast motion. The carbon NMR spectrum confirms the presence of imidazole in the sample. In summary, NMR detected one <sup>11</sup>B signal from NaBH<sub>4</sub> and two <sup>23</sup>Na signals presumably from NaBH<sub>4</sub> and NaIm. The fact that NMR spectra distinguish only two different surroundings of Na cations (having imidazolate or borohydride anions in its vicinity, respectively) clearly points out that the observed unidentified crystalline phase in the XRD pattern can only be a new polymorph of one of those phases (NaIm or NaBH<sub>4</sub>).

**Thermally Induced Structural Evolution: *In Situ* High-Temperature SR-XRPD Diffraction, Thermal Analysis, and Hot-Stage Microscopy.** In order to evaluate the temperature-induced structural features of the new crystalline form, *in situ* high-temperature diffraction measurements with synchrotron radiation have been conducted. XRPD patterns collected during a heating run from RT to 240 °C and during cooling back to RT are shown in Figure 2a, while Figure 2b shows sample composition at selected temperatures.

The as-milled sample D4 contains unreacted NaIm and NaBH<sub>4</sub> and, as already realized from the laboratory diffraction experiments, a small amount of the unidentified phase; further discussion will reveal that those reflections belong to the HT polymorph of NaIm. Between 172 and 213 °C, reflections of NaIm are slowly disappearing, whereas the diffraction lines of the HT polymorph become more pronounced, until finally it melts around 216 °C. During cooling, the HT NaIm polymorph recrystallizes below 190 °C and remains stable down to RT. Figure 3 shows an interesting effect which has been noticed during the crystallization process of the HT NaIm polymorph.

With the grain growth, diffuse scattering around the first diffraction line 100 appears, and with further cooling, pronounced streaks, instead of a defined diffraction rings, are observed, as shown in the inset in Figure 3. Such a diffuse feature is an indication of the prominent increase of defects and/or disorder within the structure. The morphology of the sample changed from fine to quite grainy (Figure S2). An attempt to solve the structure from powder data has been made on data collected at  $T = 139$  °C during the cooling cycle.

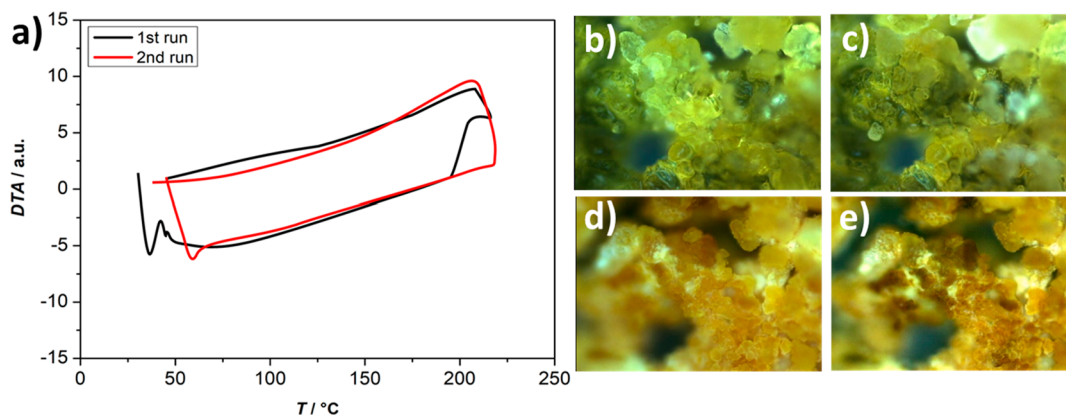


**Figure 4.** (a) DTA curves (heating and cooling) of NaIm measured in the nitrogen flow. Hot-stage microscopy images of NaIm crystals taken in the first heating run at (b) RT, (c) 180 °C, (d) 208 °C, and second heating run at (e) 210 °C.

The diffraction pattern has been indexed in the trigonal  $P3_112$  space group with cell parameters  $a = 10.3439(3)$  Å and  $c = 21.8375(1)$  Å, by the program FOX;<sup>27</sup> however, a significant overlap of diffraction peaks, as well as disorder of the structure, prevented a successful structure determination from powder data.

Furthermore, in order to additionally characterize the thermal behavior of NaIm and to precisely determine the temperature of phase transition, differential thermal analysis (DTA) was performed on the as-prepared NaIm (without the presence of borohydride) in the temperature range between room temperature and 220 °C in a stream of nitrogen gas (Figure 4a). The temperature range has been chosen to be somewhat narrower compared to *in situ* HT-PXRD measurements (220 instead of 240 °C) to avoid unnecessary melting. During the first heating run, an exothermic peak corresponding to the phase transition of the room-temperature form to the high-temperature form has been observed at  $T = 205$  °C (starting at  $\sim 188$  °C). No additional peaks were observed during the continued cooling down to RT, confirming that the high-temperature polymorph is, indeed, retained even at RT. During the second heating run, from room-temperature to 220 °C, no additional phase transitions have been noticed, pointing out to the excellent thermal stability of the second NaIm polymorph; irreversibility of the phase transition was also additionally confirmed by DSC (Figure S3).

Thermally induced phase transition was also visually detected using a hot-stage microscopy (Figure 4b–e). The room-temperature polymorph of NaIm (without the presence of  $\text{NaBH}_4$ ) was heated to 220 °C and cooled back to room temperature. This procedure was repeated in order to confirm that the results are reproducible. As can be seen from Figure 4, crystals started to slowly melt at the edges around 180 °C (Figure 4c), reshape, reorganize, and undergo a color change. Once this transformation is finished, no further change in color or shape of the crystals could be observed nor during cooling down to room temperature and neither during new heating cycles, again confirming that phase transition from the room-temperature NaIm to the high-temperature NaIm polymorph is an irreversible process. Phase composition of the sample prior and after the hot-stage microscopy measurement was confirmed by PXRD (Figure S4).

Finally, *in situ* high-temperature XRPD measurements have been performed on as-prepared NaIm (Figure 5).

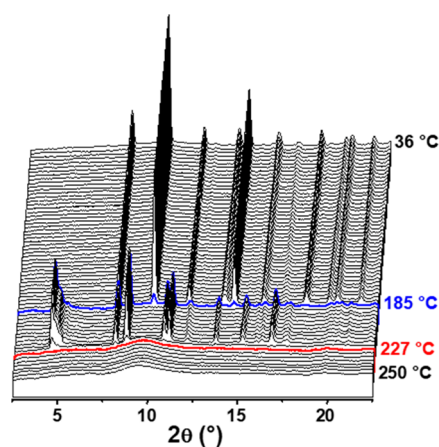


**Figure 5.** *In situ* high-temperature XRPD of NaIm measured in the temperature range  $T = 36$ – $250$  °C at  $15.6$  °C/h heating rate (using the Mo radiation).

Figure 5 shows that NaIm transforms to its high-temperature phase at 185 °C before it melts at 227 °C. The transition temperature measured by *in situ* XRPD is slightly lower than the temperature measured by thermal methods; however, this difference is not significant considering the uncertainty of temperatures measured by XRPD.

**Single Crystal Preparation and Structure Determination.** In order to determine the structure of the new NaIm polymorph, additional attempts to prepare the compound in the form of single crystals have been carried out. The experimental setup is shown in Figure S5. Pure NaIm was heated on a heating plate for 20 min in a capillary in a sand bath at  $T = 210$  °C, a temperature well above the phase transformation, followed by slow cooling down to the RT, yielding single crystals of an adequate size for the structure solution (Figure S2). Single-crystal determination revealed that the HT polymorph of NaIm crystallizes in the trigonal  $P3_112$  space group with cell parameters  $a = 10.3164(4)$  Å and  $c = 21.4192(11)$  Å, confirming that the indexing process of the powder pattern was indeed correct. The structure was solved by direct methods and refined as a twin by inversion. Besides the inversion twin, no other twinning is involved. During structure refinement, only Na1 and Na2 have been refined as fully occupied, and the remaining sodium atoms (Na3 and Na4) and all imidazolate anions are found to be disordered over two discrete sites with a 73/27 ratio (Figure 6).

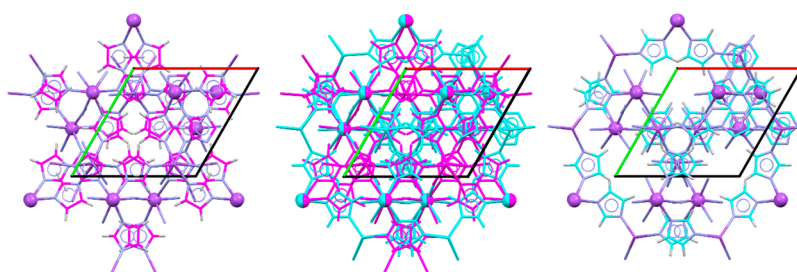


**Figure 6.** Views of both disordered parts, major part (left 73%, carbons in magenta), minor part (right 27%, carbons in cyan), and overlapped structures (center). Fully occupied Na atoms are shown as spheres.

Crystal data and summary of refinement are given in Table 1, while the crystal structure is shown in Figure 7.

**Table 1. Crystal Data and Summary of Structure Refinement for HT-NaIm**

empirical formula	$C_9H_9N_6Na_3$
formula weight	270.19
temperature (K)	250(2)
wavelength (Å)	1.54184
crystal system	trigonal
space group	$P3_112$
unit cell dimensions (Å)	$a = 10.3164(4)$ $b = 10.3164(4)$ $c = 21.4192(11)$
volume (Å <sup>3</sup> )	1974.21(18)
Z	6
density (calculated) (g/cm <sup>3</sup> )	1.364
absorption coefficient (mm <sup>-1</sup> )	1.603
$F(000)$	828
crystal size (mm <sup>3</sup> )	$0.236 \times 0.132 \times 0.077$
$\theta$ range for data collection	$4.950\text{--}69.998^\circ$
reflections collected	13271
independent reflections	2498 [ $R_{\text{int}} = 0.0401$ ]
completeness to $\theta = 67.684^\circ$	100.0%
absorption correction	Gaussian
max. and min transmission	1.000 and 0.561
data/restraints/parameters	2498/120/288
goodness-of-fit on $F^2$	1.098
final R indices [ $I > 2\sigma(I)$ ]	$R_1 = 0.0516$ , $wR_2 = 0.1460$
R indices (all data)	$R_1 = 0.0682$ , $wR_2 = 0.1619$
absolute structure parameter	0.6(4) (twin by inversion)
largest diff. peak and hole	0.190 and $-0.245 \text{ e}\cdot\text{Å}^{-3}$

The HT-NaIm structure contains four independent sodium atoms. Sodium atoms Na2 and Na4 are octahedrally coordinated by six imidazolates via their nitrogen atoms. Atoms Na1 and Na3 are connected to N atoms from three imidazolates, while the additional fourth imidazolate ring forms a metal- $\pi$  interaction as shown in Figure 7a. Figure 7b shows two different chains both having the  $3_1$  screw axis along the  $c$ -direction. The first chain contains fully occupied Na1 and Na2 atoms, while, in the second chain, only the partially occupied Na3 and Na4 atoms are present. Those chains are mutually connected as shown in Figure 7c. The repeating sequence in each chain can be described as a trimeric unit with formula  $Na_3Im_6$ . The trimeric unit in the case of the first chain consists of two Na1 tetrahedra and one Na2 octahedron connected in the face-shared manner and two Na3 octahedra and one Na4 tetrahedron in the case of the second chain.

Unlike the low-temperature NaIm polymorph, which shows a tetrahedral coordination of the sodium atom, in the structure of the HT-NaIm polymorph, the sodium atoms exhibit both tetrahedral coordination as well as a distorted octahedral coordination. The interatomic distances around the tetrahedrally coordinated sodium atoms, in the range  $d(Na_{\text{tet}} - N_{\text{Im}})_{\text{HT-NaIm}} = 2.374\text{--}2.461 \text{ \AA}$ , are found to be a bit shorter in the case of the high-temperature polymorph of NaIm compared to the RT polymorph [ $d(Na_{\text{tet}} - N_{\text{Im}})_{\text{NaIm}} = 2.403\text{--}2.514 \text{ \AA}$ ]. The interatomic distances in the case of octahedrally coordinated sodium atoms are longer [ $d(Na_{\text{oct}} - N_{\text{Im}})_{\text{HT-NaIm}} = 2.525\text{--}2.703 \text{ \AA}$ ] compared to sodium atoms showing a tetrahedral coordination as expected for higher coordination number.

Crystal packing of HT-NaIm is characterized by the presence of cavities around the  $3_1$  axis. The cavities are shown in Figure 8 as green spheres. Considering the major and minor parts on their own, Platon<sup>28</sup> calculates the volume of these voids as 50 and 53 Å<sup>3</sup> for the major and minor part, respectively. In both cases, the cavities occupy ca. 8% of the unit cell volume.

Figure 9 shows the hexagonal planes containing the triplet of coordination polyhedra. The planes are packed along the  $c$ -axis in hexagonal close packing (HCP) (gray-magenta or gray-cyan) with cubic close packed (CCP) domains (gray-magenta-cyan). This is a typical example of stacking faults between HCP and CCP, which explains also the diffuse streaks observed on diffraction pattern images of the single crystal on cooling.

## CONCLUSION

In conclusion, reactivity and stability of metal imidazolates differ significantly within the group of alkali elements. Contrary to lithium, sodium imidazolate in the reaction with sodium borohydride does not form a hybrid compound; instead, a high-temperature polymorph of NaIm appears. It is important to highlight that HT-NaIm has been identified during the mechanochemical reaction of NaIm (in excess) with  $NaBH_4$ , which means that a simple mechanochemical reaction of the RT polymorph can induce the phase transformation to the high-temperature form. Nevertheless, it seems that milling-induced phase transition of NaIm is not a straightforward process and that it is dependent on the amount of  $NaBH_4$  present in the system. One would expect that the largest amount of HT-NaIm will be observed when the starting amount of NaIm is the highest, i.e., in the case when NaIm is used in excess compared to  $NaBH_4$ , but in fact, quantitative Rietveld refinements (Figure S1) showed that the highest amount of NaIm has been transformed to the high-temperature polymorph when the ratio of  $NaBH_4$ :NaIm = 1:4 (not

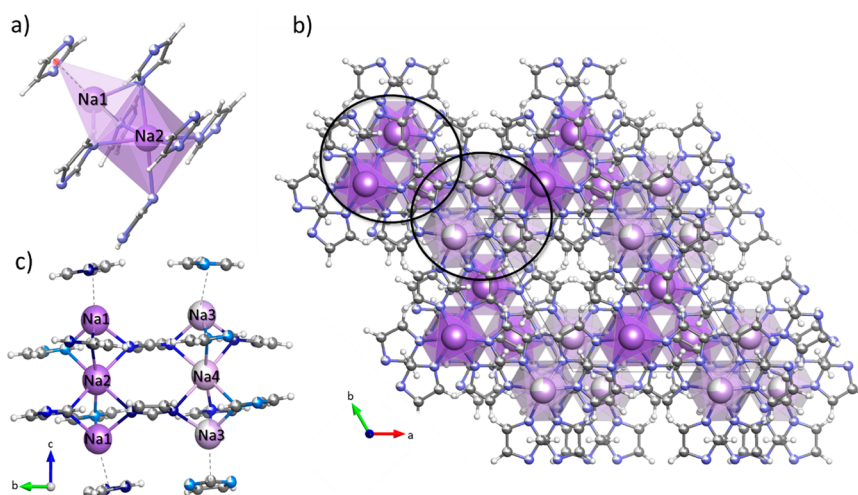


**Figure 7.** (a) Octahedral coordination of Na2 atom and tetrahedral coordination of Na1 formed by three imidazolate nitrogen atoms and the centroid (in red) of a fourth imidazolate. (b) Two chains with 3<sub>1</sub> screw axis viewed along the *c*-direction shown in two different shades of purple; darker polyhedra show the chain with fully occupied sodium atoms (Na1 and Na2), while the helix with partially occupied sodium atoms (Na3 and Na4) is given by lighter shade of purple polyhedra. (c) Mutually interconnected chains running parallel to the *c*-axis. Three types of imidazole rings, exhibiting different surroundings, are shown by three shades of blue.

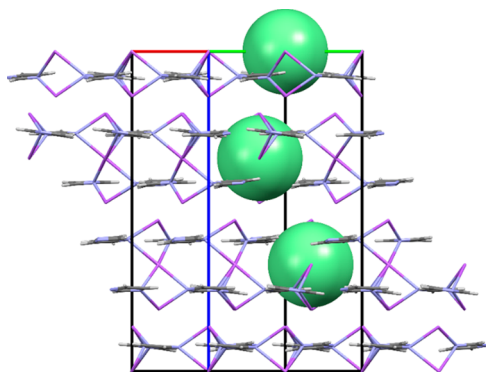


**Figure 8.** Crystal voids shown as green spheres, symmetry related by a 3<sub>1</sub> axis. The origin of the spheres lies on the centroid of the cavity, and the radius was chosen to approximate the calculated void volume.

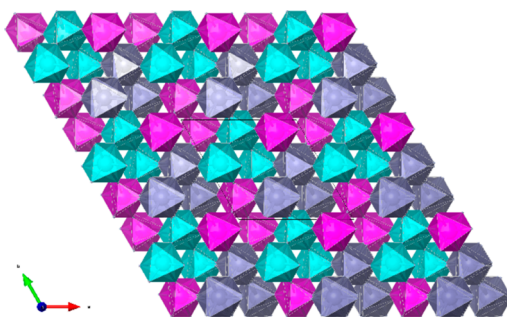


**Figure 9.** 3D framework of HT-NaIm in the *ab* plane. Helical chains containing fully occupied Na positions are given in gray, while the majority and the minority helices are given in magenta and cyan, respectively.

the 1:6 ratio, as might be expected). Furthermore, it must be noted that, while the HT-NaIm can be obtained by neat-grinding, DMSO or ACN assisted grinding does not result in the phase transformation to the high-temperature form (Figure S6, Table S1). The high-temperature polymorph of NaIm crystallizes with heating also in other reactions starting from

NaIm and metal borohydride ( $\text{Mg}(\text{BH}_4)_2$ ,  $\text{Mn}(\text{BH}_4)_2$ ) (Figures S7 and S8).

Additionally, the pure HT polymorph has been prepared by simple heating of RT-NaIm at 210 °C. From the results obtained by DTA analysis, as well as those from hot-stage microscopy, the irreversible polymorphic transformation from room-temperature to high-temperature polymorph has been confirmed. After RT-NaIm is transformed into the high-temperature polymorph at 205 °C, no reversibility of transformation to RT-NaIm has been observed upon cooling to RT. Generally, one might expect that a densely packed structure, such as the structure of the RT polymorph, is more stable compared to the polymorphic phase that is loosely packed; however, this demonstrates, as in many examples known in the literature,<sup>12–15</sup> that the conversion to the stable polymorphic phase can easily be hindered due to the slow kinetics of the phase transition. The fact that the HT phase exhibits a porous framework structure and, moreover, remains stable upon cooling to RT suggests possible application of this material for gas sorption/separation.

## ■ ASSOCIATED CONTENT

### SI Supporting Information

The Supporting Information is available free of charge at <https://pubs.acs.org/doi/10.1021/acs.cgd.0c01006>.

Reactants used for the mechanochemical synthesis (Table S1), Rietveld refinement of samples D1–D7 (Figure S1), sample D4 transformed from powder to grainy (Figure S2), DSC curves of NaIm on heating and cooling (Figure S3), Rietveld refinement of NaIm before and after hot-stage microscopy experiment (Figure S4), experimental setup for the crystallization of high-temperature NaIm polymorph (Figure S5), Rietveld refinements for samples S1 and S2 (Figure S6), quantitative composition of crystalline products in samples S1 and S2 (Table S2), XRD patterns of sample prepared from NaIm and  $\text{Mg}(\text{BH}_4)_2$  in ratio 6:1 (Figure S7), XRD patterns of sample prepared from NaIm and  $\text{Mn}(\text{BH}_4)_2$  in ratio 6:1 (Figure S8) (PDF)

### Accession Codes

CCDC 2014750 contains the supplementary crystallographic data for this paper. These data can be obtained free of charge via [www.ccdc.cam.ac.uk/data\\_request/cif](http://www.ccdc.cam.ac.uk/data_request/cif), or by emailing [data\\_request@ccdc.cam.ac.uk](mailto:data_request@ccdc.cam.ac.uk), or by contacting The Cambridge Crystallographic Data Centre, 12 Union Road, Cambridge CB2 1EZ, UK; fax: +44 1223 336033.

### AUTHOR INFORMATION

#### Corresponding Author

Jasminka Popović – Laboratory for Synthesis and Crystallography of Functional Materials, Division for Materials Physics, Ruđer Bošković Institute, HR-10000 Zagreb, Croatia; [orcid.org/0000-0003-0800-2249](https://orcid.org/0000-0003-0800-2249); Email: [Jasminka.Popovic@irb.hr](mailto:Jasminka.Popovic@irb.hr)

#### Authors

Sanja Burazer – Laboratory for Synthesis and Crystallography of Functional Materials, Division for Materials Physics, Ruđer Bošković Institute, HR-10000 Zagreb, Croatia; [orcid.org/0000-0002-5266-5827](https://orcid.org/0000-0002-5266-5827)

Koen Robeyns – Institute of Condensed Matter and Nanosciences, Université catholique de Louvain, 1348 Louvain-la-Neuve, Belgium

Laure Guéneau – Laboratory of Crystallography, DQMP, University of Geneva, CH-1211 Geneva, Switzerland

Gregor Mali – Department of Inorganic Chemistry and Technology, National Institute of Chemistry, SI-1001 Ljubljana, Slovenia; [orcid.org/0000-0002-9012-2495](https://orcid.org/0000-0002-9012-2495)

Fabrice Morelle – Institute of Condensed Matter and Nanosciences, Université catholique de Louvain, 1348 Louvain-la-Neuve, Belgium

Voraksmy Ban – Institute of Condensed Matter and Nanosciences, Université catholique de Louvain, 1348 Louvain-la-Neuve, Belgium; [orcid.org/0000-0002-8820-503X](https://orcid.org/0000-0002-8820-503X)

Teodoro Klaser – Department of Physics, Faculty of Science, University of Zagreb, HR-10000 Zagreb, Croatia

Yaroslav Filinchuk – Institute of Condensed Matter and Nanosciences, Université catholique de Louvain, 1348 Louvain-la-Neuve, Belgium; [orcid.org/0000-0002-6146-3696](https://orcid.org/0000-0002-6146-3696)

Radovan Černý – Laboratory of Crystallography, DQMP, University of Geneva, CH-1211 Geneva, Switzerland; [orcid.org/0000-0002-9847-4372](https://orcid.org/0000-0002-9847-4372)

Complete contact information is available at: <https://pubs.acs.org/10.1021/acs.cgd.0c01006>

### Notes

The authors declare no competing financial interest.

### ACKNOWLEDGMENTS

The authors acknowledge the financial support of the Swiss National Science Foundation in the scope of Joint Research Projects (SCOPES) under the title “Metal-Hydride Organic Frameworks (HOF) - new solids for gas adsorption and separation”. S.B. and J.P. acknowledge the financial support of the Croatian Science Foundation in the scope of “Development of early stage researchers carriers - education of new PhD students”. This work was supported by FNRS (FRIA scholarship allocated to F.M., PDR T.0169.13, EQP U.N038.13, J.0164.17). The authors acknowledge the Swiss-

Norwegian Beamlines of ESRF for the allocation of beamtime and excellent support with the data collection.

### REFERENCES

- (1) Safin, D. A.; Robeyns, K.; Filinchuk, Y. Magnesium imidazolate - a first porous zeolitic imidazolate framework with alkali and alkaline earth metals. *Acta Crystallogr., Sect. A: Found. Adv.* **2016**, *72* (a1), s402.
- (2) Park, K. S.; Ni, Z.; Côté, A. P.; Choi, J. Y.; Huang, R.; Uribe-Romo, F. J.; Chae, H. K.; O’Keeffe, M.; Yaghi, O. M. Exceptional chemical and thermal stability of zeolitic imidazolate frameworks. *Proc. Natl. Acad. Sci. U. S. A.* **2006**, *103*, 10186–10191.
- (3) Yang, J.; Zhang, Y.-B.; Liu, Q.; Trickett, C. A.; Guetierrez-Puebla, E.; Monge, M. A.; Cong, H.; Aldossary, A.; Deng, H.; Yaghi, O. M. Principles of designing extra-large pore openings and cages in zeolitic imidazolate frameworks. *J. Am. Chem. Soc.* **2017**, *139*, 6448–6455.
- (4) Eberle, U.; Felderhoff, M.; Schüth, F. Chemical and physical solutions for hydrogen storage. *Angew. Chem., Int. Ed.* **2009**, *48*, 6608–6630.
- (5) Suh, M. P.; Park, H. J.; Prasad, T. K.; Lim, D.-W. Hydrogen storage in metal-organic frameworks. *Chem. Rev.* **2012**, *112*, 782–835.
- (6) Thomas, K. M. Hydrogen adsorption and storage on porous materials. *Catal. Today* **2007**, *120*, 389–398.
- (7) Farha, O. K.; Yazaydin, A. O.; Eryazici, I.; Malliakas, C. D.; Hauser, B. G.; Kanatzidis, M. G.; Nguyen, S. T.; Snurr, R. Q.; Hupp, J. T. De novo synthesis of a metal-organic framework material featuring ultrahigh surface area and gas storage capacities. *Nat. Chem.* **2010**, *2*, 944–948.
- (8) Furukawa, H.; Ko, N.; Go, Y. B.; Aratani, N.; Choi, S. B.; Choi, E.; Yazaydin, A. O.; Snurr, R. Q.; O’Keeffe, M.; Kim, J.; Yaghi, O. M. Ultrahigh porosity in metal-organic frameworks. *Science* **2010**, *329*, 424–428.
- (9) Kaye, S. S.; Dailly, A.; Yaghi, O. M.; Long, J. R. Impact of preparation and handling on the hydrogen storage properties of Zn<sub>4</sub>O(1,4-benzenedicarboxylate)<sub>3</sub> (MOF-5). *J. Am. Chem. Soc.* **2007**, *129*, 14176–14177.
- (10) *Project Metal-Hydride Organic Frameworks (HOF)-new solids for gas adsorption and separation*; Vinča Institute of Nuclear Sciences, University of Belgrade: Belgrade, Serbia, 2015.
- (11) Morelle, F.; Ban, V.; Filinchuk, Y. Towards hydridic nanoporous frameworks: the first imidazolate-borohydride compound Li<sub>2</sub>ImBH<sub>4</sub> (Im = [C<sub>3</sub>H<sub>3</sub>N<sub>2</sub>]<sup>-</sup>). In *14th International Symposium on Metal-Hydrogen Systems (MH2014)*; Manchester, U.K., July 20–25, 2014; ThOQ:128.
- (12) Skripov, A. V.; Dimitrievska, M.; Babanova, O. A.; Skoryunov, R. V.; Soloninin, A. V.; Morelle, F.; Filinchuk, Y.; Faraone, A.; Wu, H.; Zhou, W.; Udovic, T. J. Low-temperature rotational tunneling of tetrahydridoborate anions in lithium benzimidazolate-borohydride Li<sub>2</sub>(bIm)BH<sub>4</sub>. *J. Phys. Chem. C* **2019**, *123*, 20789–20799.
- (13) Bernstein, J. Crystal Polymorphism. In *Engineering of Crystalline Materials Properties*; Novoa, J. J., Braga, D., Addadi, L., Eds.; NATO Science for Peace and Security Series B: Physics and Biophysics; Springer Netherlands: Dordrecht, 2008; pp 87–109.
- (14) Androš, L.; Jurić, M.; Popović, J.; Santić, A.; Lazić, P.; Benčina, M.; Valant, M.; Brničević, N.; Planinić, P. Ba<sub>4</sub>Ta<sub>2</sub>O<sub>9</sub> Oxide Prepared from an Oxalate-Based Molecular Precursor-characterization and Properties. *Inorg. Chem.* **2013**, *52*, 14299–14308.
- (15) Filipovich, V. N.; Kalinina, A. M. In *The Structure of Glass*, Vol. 5; Torapov, N. A., Porai-Koshits, E. A., Eds.; Consultants Bureau: New York, 1965; p 34.
- (16) Garvie, R. C. Stabilization of the tetragonal structure in zirconia microcrystals. *J. Phys. Chem.* **1978**, *82*, 218–224.
- (17) Shukla, S.; Seal, S.; Vij, R.; Bandyopadhyay, S.; Rahman, Z. Effect of nanocrystalline morphology on the metastable tetragonal phase stabilization in zirconia. *Nano Lett.* **2002**, *2*, 989–993.
- (18) Skoko, Ž.; Zamir, S.; Naumov, P.; Bernstein, J. The Thermosalient Phenomenon. “Jumping Crystals” and Crystal

Chemistry of the Anticholinergic Agent Oxitropium Bromide. *J. Am. Chem. Soc.* **2010**, *132*, 14191–14202.

(19) Morelle, F. Hybrid hydridic frameworks by the combination of complex hydrides and nitrogen-based organic ligands. Ph.D. Dissertation, Université catholique de Louvain, Louvain-la-Neuve, Belgium, 2017.

(20) Burazer, S.; Morelle, F.; Filinchuk, Y.; Černý, R.; Popović, J. Mixed-metal imidazolates containing alkali and alkaline earth metals: Mechanochemical synthesis and crystal structure of AMgIm<sub>3</sub> (A = Na or K). *Inorg. Chem.* **2019**, *58*, 6927–6933.

(21) Hammersley, A. P.; Svensson, S. O.; Hanfland, M.; Fitch, A. N.; Häusermann, D. Two-dimensional detector software: From real detector to idealised image or two-theta scan. *High Pressure Res.* **1996**, *14*, 235–248.

(22) Dyadkin, V.; Pattison, Ph.; Dmitriev, V.; Chernyshov, D. A new multipurpose diffractometer PILATUS@SNBL. *J. Synchrotron Radiat.* **2016**, *23*, 825.

(23) *CrysAlisPro*, ver. 1.171.38.46; Rigaku Oxford Diffraction, 2015.

(24) Sheldrick, G. M. SHELXT - Integrated space-group and crystalstructure determination. *Acta Crystallogr., Sect. A: Found. Adv.* **2015**, *A71*, 3–8.

(25) Momma, K.; Izumi, F. VESTA 3 for three-dimensional visualization of crystal, volumetric and morphology data. *J. Appl. Crystallogr.* **2011**, *44*, 1272–1276.

(26) Macrae, C. F.; Edgington, P. R.; McCabe, P.; Pidcock, E.; Shields, G. P.; Taylor, R.; Towler, M.; van de Streek, J. Mercury: Visualization and analysis of crystal structures. *J. Appl. Crystallogr.* **2006**, *39*, 453–457.

(27) Favre-Nicolin, V.; Cerny, R. "Free Objects for Crystallography": a modular approach to ab initio structure determination from powder diffraction. *J. Appl. Crystallogr.* **2002**, *35*, 734–743.

(28) Spek, A. L. Single-crystal structure validation with the program PLATON. *J. Appl. Crystallogr.* **2003**, *36*, 7–13.